Effect of non-thermal plasma in the activation and regeneration of 13X zeolite for enhanced VOC elimination by cycled storage and discharge process

S. K. P. Veerapandian, N. de Geyter, Jean-Marc Giraudon, Jean-Charles Morin, P. S. E. Tabaei, G. de Weireld, A. Laemont, K. Leus, P. van der Voort, Jean-Francois Lamonier, et al.

▶ To cite this version:

S. K. P. Veerapandian, N. de Geyter, Jean-Marc Giraudon, Jean-Charles Morin, P. S. E. Tabaei, et al.. Effect of non-thermal plasma in the activation and regeneration of 13X zeolite for enhanced VOC elimination by cycled storage and discharge process. Journal of Cleaner Production, 2022, 364 (132687), 10.1016/j.jclepro.2022.132687 . hal-04053366

HAL Id: hal-04053366
https://hal.univ-lille.fr/hal-04053366v1

Submitted on 31 Mar 2023

Effect of non-thermal plasma in the activation and regeneration of 13X zeolite for enhanced VOC elimination by cycled storage and discharge process

Savita Kaliya Perumal Veerapandian[1], Nathalie De Geyter[1], Jean-Marc Giraudon[2], Jean-Charles Morin[2], Parinaz Saadat Esbah Tabaei[1], Guy De Weireld[3], Andreas Laemont[4], Karen Leus[4], Pascal Van Der Voort[4], Jean-François Lamonier[2] and Rino Morent[1]

[1] Ghent University, Faculty of Engineering and Architecture, Department of Applied Physics, Research Unit Plasma Technology, Sint-Pietersnieuwstraat 41 B4, 9000 Ghent, Belgium

*(*email: savita.kaliyaperumalveerapandian@ugent.be)*

[2] Univ. Lille, CNRS, Centrale Lille, Univ. Artois, UMR 8181 – UCCS – Unité de Catalyse et Chimie du Solide, F-59000 Lille, France

[3] Université de Mons, Faculté Polytechnique, Service de Thermodynamique et de Physique Mathématique, Place du Parc, 20, 7000 Mons, Belgium

[4] Ghent University, Department of Chemistry, COMOC-Center for Ordered Materials, Organometallics and Catalysis, Krijgslaan 281-S3, 9000 Ghent, Belgium

Abstract.

A non-thermal plasma (NTP) discharge is used in this study for the activation and regeneration of MS-13X pellets packed in a MS-13X & glass beads packed bed dielectric barrier discharge (DBD) reactor. NTP activation (*in-situ*) of MS-13X efficiently removes the adsorbed carbonaceous compounds and moisture resulting in an improved VOC adsorption. In addition, NTP exposure is used for the regeneration of the used MS-13X for cycled storage and discharge (CSD) removal of VOC from air. The amount of adsorbed toluene, products formed and the surface and bulk properties of the regenerated used MS-13X shows complete regeneration of used MS-13X. Finally, the stability of MS-13X during 10 cycles of CSD shows no degradation in performance. Thus, NTP exposure is proven to be successful for both the activation and regeneration of MS-13X pellets used for cyclic CSD process.

Keywords: MS-13X, NTP activation, NTP regeneration, VOC abatement, Cycled storage and discharge

Number of words: 6591

1. Introduction

Most volatile organic compounds (VOCs) are toxic to human and environmental health [1]. Due to their negative impact, it is important to reduce the emission of VOCs. Among the various environmental processes which are used for the removal of VOCs from exhaust gases [2,3], adsorption is one of the most cost effective and simplest process. The most commonly used adsorbents for VOC removal are carbon based [4], and metal oxide-based adsorbents. However, the main limitations of adsorption are the need for continuous regeneration of the used adsorbent, the disposal of spent adsorbents and the processing of the adsorbed VOCs. In practice, most saturated sorbents are either incinerated or disposed which leads to a negative impact on the environment. To make the adsorption process more environmentally friendly and to reduce the demand for virgin adsorbents, it is thus indispensable to regenerate the used adsorbents. Several processes which have been investigated for the regeneration of adsorbents include pressure swing [5], temperature swing [6], microwave heating [6,7], purging gas [6], chemical methods [5], and the combination of heating and catalytic oxidation [8]. In addition, non-thermal plasmas (NTPs) have also been proven effective for the regeneration of spent adsorbents [9,10], as NTPs generate ozone and N_2O which are very effective oxidizing agents.

Important adsorbent properties which have to be considered for pollution control include pore size distribution, surface area, thermal stability and hydrophobicity. Due to their large specific surface area, narrow pore size distribution and acidity, zeolites are very interesting candidates as adsorbents [11]. In this particular work, zeolite X is used as adsorbent which is commercially available as MS-13X (molecular sieve) in sodium (mostly) and calcium form. Zeolite 13X is a faujasite (FAU) molecular sieve with a 3D pore structure, a pore size of ~ 7 Å and an Si/Al ratio of ~2.6-3. The pore size of MS-13X is suitable for the adsorption of various VOCs such as hexane, toluene, benzene, ethyl benzene, o-, m-, p- xylene and methyl ethyl ketone (kinetic diameter in the range of 4.3 - 6.8 Å) [12–14] and also accessible for ozone (kinetic diameter of 5.8 Å) [15] which is one of the oxidizing species produced by an NTP.

This paper deals with the engineering of an original environmental process which combine (i) adsorption and (ii) plasma discharge, which is known as a cycled storage and discharge (CSD) process for the removal of VOCs from air. This environmental process involves two steps: first, the diluted VOC is concentrated on the adsorbent (plasma off). Then, the adsorbed VOC is oxidized by NTP discharge. The advantages of this process are: (i) reduced energy consumption by increasing the ratio of the adsorption time to the plasma discharge time (particularly suitable for low concentration of VOC in a large volume of exhaust gas), (ii) simultaneous oxidation of the adsorbed VOC and regeneration of the adsorbent, avoids an extra step of regeneration and (iii) the possibility to use a benign discharge gas which avoids the formation of unwanted and toxic by-products such as NO_x (which is out of scope for this work).

In the past, Chao et al. investigated the decomposition of toluene using ozone in the presence of 13X zeolite [16] and reported the enhanced degradation of toluene, as the Lewis acid sites of the zeolite decomposed ozone to form active oxygen which has a higher reactive rate constant when compared to ozone [17]. However, the deactivation of the 13X zeolite occurred after a few hours of experiments. Yi et al. investigated a metal loaded 13X zeolite for the removal of toluene using adsorption plasma catalysis (APC) and reported that the catalytic activity and product selectivity were improved by the metal loading [18]. In addition, Yi et al. also investigated the effect of a closed and ventilated discharge on the oxidation of toluene adsorbed on a Co/13X zeolite and reported that the closed discharge was more efficient for the oxidation of toluene [19]. Researchers investigated the use of bare 13X and metal loaded 13X for the removal of various VOCs such as ethylene [20,21], benzene [22,23] and toluene [23]. Researchers also investigated the use of different catalysts such as $Mn\text{-}Cu/Al_2O_3$ [24] and $CeO_2\text{-}Co_3O_4/\gamma\text{-}Al_2O_3$ [25] for APC abatement of VOCs.

Although the above-mentioned research works established the use of MS-13X or metal loaded MS-13X for APC or CSD removal of VOCs, these works have never investigated the effect of the used NTP discharge on the surface and bulk properties of adsorbents in detail, which is critical for CSD process. Apart from the stability of adsorbent in NTP discharge, the regenerability of adsorbent by NTP has to be investigated as well. Thus, the main objective of this work is to investigate the use of an NTP sustained in dry air for the activation of fresh MS-13X and the regeneration of used MS-13X for CSD removal of toluene, a model VOC.

In the first part of this work, the adsorption capacity of MS-13X pellets activated by heating and NTP discharge is compared. In the second part of this work, the use of NTP for the simultaneous oxidation of adsorbed toluene and the regeneration of MS-13X pellets is studied. Then, the surface and bulk properties of thermal activated, NTP activated and NTP regenerated MS-13X are studied. Based on the obtained results, correlations between the physico-chemical properties and the adsorption capacity of MS-13X pellets activated by different methods are discussed. To the best of our knowledge, this is the first work which investigates the use of NTP discharge for both the activation and *in-situ* regeneration of adsorbents and the effect of NTP discharge on the surface and bulk physicochemical properties of adsorbents.

2. Experimental methods

2.1 Experimental set-up

The general schematic representation of the experimental set-up used for the activation of MS-13X and the CSD process is shown in Figure S1. The experimental set-up comprises a gas supply system, MS-13X pellets and glass beads packed bed DBD reactor (shown in Figure S2) and analytical instrumentation for flue gas analysis. The detailed description of the experimental set-up is given in the supplementary information and elsewhere [26].

2.2 Activation of MS-13X

To remove the adsorbed carbonaceous compounds and moisture, the purchased MS-13X pellets is usually heated to high temperatures prior to adsorption [27]. In this work, MS-13X pellets was activated using two different methods: (i) by heating and (ii) by NTP exposure. Thermal activation was carried out by heating MS-13X in a flow of dry air (0.2 $L^{\cdot}min^{-1}$) from room temperature to 400˚C at a heating rate of 1˚C/min and maintained at 400°C for 4 hours [28]. NTP activation was carried out in the DBD reactor using a fixed flow of dry air of 0.5 $L^{\cdot}min^{-1}$ for 1 hour using different discharge powers (between 6 and 65 W). The MS-13X samples activated by heating and NTP are labelled as “thermal activated” and “NTP activated”, respectively.

2.3 Cycled storage and discharge process

A schematic representation of the different steps in a CSD for the abatement of toluene in dry air is reported elsewhere [9]. The three steps of each cycle of CSD are: (i) the adsorption of toluene on activated MS-13X pellets either until saturation or until a certain critical concentration of toluene is reached, (ii) the desorption of reversibly adsorbed toluene by flushing with dry air and (iii) NTP exposure for the oxidation of irreversibly adsorbed toluene and the regeneration of MS-13X for the next cycle of adsorption. The experimental parameters used during the different steps of the CSD process for the abatement of toluene are summarized in Table S2.

The MS-13X samples activated by heating and NTP are labelled as "thermal activated" and "NTP activated", respectively. The NTP regenerated MS-13X is labelled as "NTP (X) regenerated", where X corresponds to the number of exposure times to the NTP discharge in addition to the activation (in case of NTP activation).

2.4 Catalyst characterization

The fresh, thermal activated, NTP activated and NTP (II) regenerated MS-13X samples were characterized using different techniques including powder X-ray diffraction (PXRD), X-ray photoelectron spectroscopy (XPS), nitrogen adsorption-desorption analysis, argon sorption and pyridine-Fourier transform infrared spectroscopy (py-FTIR) [29].

2.5 Stability tests

To examine the stability of the zeolite used in this work, 1000 ppm of toluene in dry air (flow rate = 0.1 L/min) was first adsorbed on NTP activated MS-13X until the concentration of toluene in the outlet of the plasma reactor was 10% of the initial concentration. After flushing with dry air, the NTP was turned on for 60 minutes to oxidize the irreversibly adsorbed toluene and to regenerate the MS-13X. This sequence of CSD was repeated for 10 cycles. In addition, the regeneration efficiency (RE) defined as the ratio of the adsorption capacity of the NTP regenerated MS-13X ($[Toluene]_{adsorbed,reg}$) to that of the fresh NTP activated MS-13X ($[Toluene]_{adsorbed,fresh}$) was also calculated.

3. Results and Discussion

3.1 Activation of 13X zeolite

The breakthrough curves of toluene adsorbed on thermal and NTP activated MS-13X are shown in Figure 1 and the amount of adsorbed toluene is determined to be 2.19 ± 0.06 and 2.45 ± 0.06 mmol/g, respectively. These results reveal that the amount of toluene adsorbed on NTP activated MS-13X is ~10% higher than on thermal activated MS-13X. In addition, the time required to reach the critical concentration of toluene in the outlet of the NTP reactor is delayed by 1 hour and 45 minutes for the NTP activated MS-13X. Moreover, the NTP activation of MS-13X is energy efficient as the power consumption of the NTP activation is at least five times lower than the thermal activation.

During thermal activation, the main products desorbed from the MS-13X are H_2O and CO_2, whereas during NTP activation, CO_2, H_2O and N_2O are the main products observed. In NTP activation, the adsorbed carbonaceous compounds are desorbed as CO_2 from MS-13X pores either by the reaction with diffused short-lived [30] or long-lived species such as O_3 and N_2O formed in NTP discharge and the adsorbed moisture is desorbed by electropolarization [31]. The amounts of CO_2 desorbed during thermal activation and NTP activation using different applied voltages, shown in Table 1, suggest that the amount of CO_2 desorbed during activation is proportional to the amount of toluene adsorbed on MS-13X. The NTP activation of the MS-13X is performed *in-situ*, whereas the thermal activation is performed *ex-situ* and transferred to the NTP reactor for toluene adsorption. It has been widely reported in literature that 13X zeolite is an efficient adsorbent material for CO_2 owing to its higher pore volume and suitable pore diameter [32] and its low Si/Al ratio with a cation which exhibits strong electrostatic attraction for CO_2 [33]. Thus, the reason for the higher adsorption of toluene from dry air on NTP activated MS-13X using applied voltages $\geq$ 7.00 kV could be as follows: (i) the amount of CO_2 desorbed by thermal activation is lower than by NTP activation at applied voltages $\geq$ 7.00 kV (see Table 1) and (ii) adsorption of CO_2 from the atmosphere can occur on the thermal activated sample as it was transferred to the NTP reactor. Thus, in order to investigate the above-mentioned possibilities, the thermal activated sample was also exposed to the NTP. During NTP exposure, more CO_2 and H_2O were desorbed, which can explain the reduced toluene adsorption on the only thermal activated MS-13X.

Thus, NTP activation of MS-13X pellets is more efficient in the removal of adsorbed carbonaceous compounds and moisture and in addition, it eliminates an extra step of sample transfer.

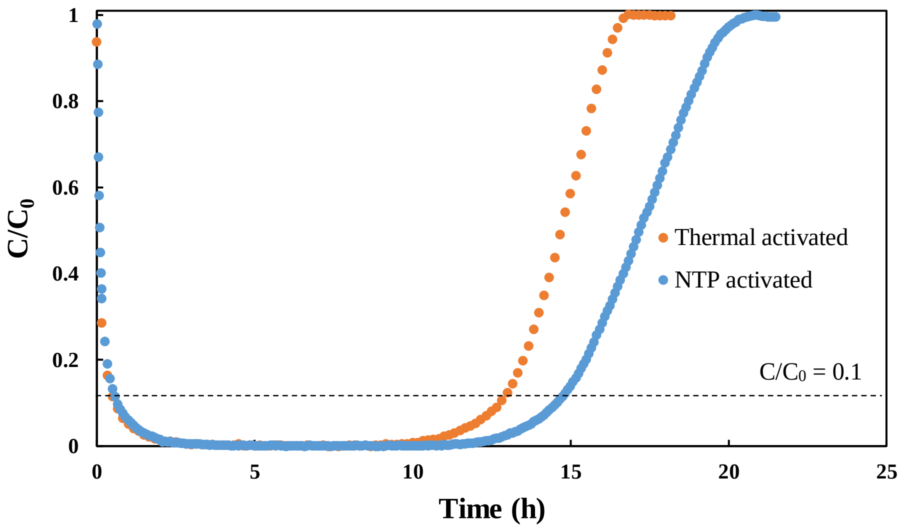

Figure 1 Adsorption of toluene in dry air (initial concentration=1000 ppm; total flow rate=0.1 L/min) on thermal activated and NTP activated MS-13X (applied voltage=7.25 kV; discharge power=58 W; plasma exposure time=1h)

Table 1 Amount of CO_2 desorbed during activation of MS-13X, amount of toluene adsorbed on activated MS-13X and time to reach the critical concentration of toluene in the outlet of the reactor during adsorption for thermal activated and NTP activated MS-13X (plasma exposure time=1 h)

	Applied voltage (kV)	Discharge power (W)	$[CO_2]_{desorbed}$ (10th min) (ppm)	$[CO_2]_{total}$ desorbed (mmol/g)	$[Toluene]_{total}$ adsorbed (mmol/g)	$T_{critical}$ conc (h)
Thermal activated	NA	NA	NA	0.09	2.19 ± 0.06	12.8
NTP activated	6.75	6	43	0.07	0.93 ± 0.03	5.5
	7.00	39	97	0.10	2.22 ± 0.12	12.5

	7.25	58	192	0.15	2.45 ± 0.06	14.6
	7.50	65	498	0.14	2.46 ± 0.09	14.3

The FTIR spectra of the outlet gas after 10 minutes of NTP exposure for various applied voltages are shown in Figure S3, in order to visualize the effect of the applied voltage on the amount of CO_2 desorbed at a given time. The amount of desorbed CO_2 after 10 minutes increases upon increasing the applied voltage (Table 1 and Figure S3). When the applied voltage increases, the discharge power increases and thus, the energy deposited on MS-13X increases resulting in more desorbed CO_2 after 10 minutes of NTP exposure.

To further investigate the effect of the applied voltage on the activation of MS-13X, the toluene adsorption capacity of NTP activated MS-13X using different applied voltages was also studied and the breakthrough curves are shown in Figure 2. The amount of toluene adsorbed (mmol/g) and the time required to reach the critical concentration of toluene in the outlet of the NTP reactor are shown in Table 1, follow the same trend as that of the total amount of CO_2 desorbed from the MS-13X during NTP activation. Considering that a lower discharge power (58 W) used for activation of MS-13X results in a similar toluene adsorption capacity (approximately 2.45 mmol/g), MS-13X activated by NTP during 1 h at an applied voltage of 7.25 kV will be used further on in this study for the investigation of CSD for the removal of toluene.

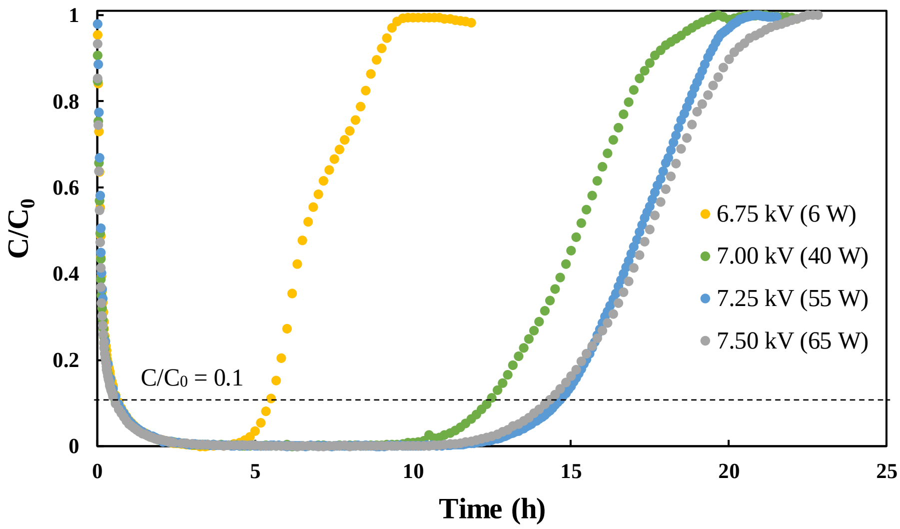

Figure 2 Effect of the applied voltage (and discharge power) during plasma activation on the adsorption of toluene from dry air on NTP activated MS-13X (flow rate=0.1 L/min; initial toluene concentration=1000 ppm; plasma exposure time=1 h)

3.2 Cycled storage and discharge process

3.2.1 Adsorption/desorption of toluene on NTP activated MS-13X

The breakthrough curve of toluene adsorbed on NTP activated MS-13X at 7.25 kV followed by the desorption of reversibly adsorbed toluene by flushing dry air is shown in Figure 3. The amount of toluene adsorbed and the amount of toluene which is reversibly adsorbed on the MS-13X sample are quantified to be 2.45 ± 0.06 mmol/g and 0.12 mmol/g, respectively. Thus, after flushing with dry air at room temperature 2.33 ± 0.05 mmol/g of toluene is still adsorbed on the surface of the NTP activated MS-13X.

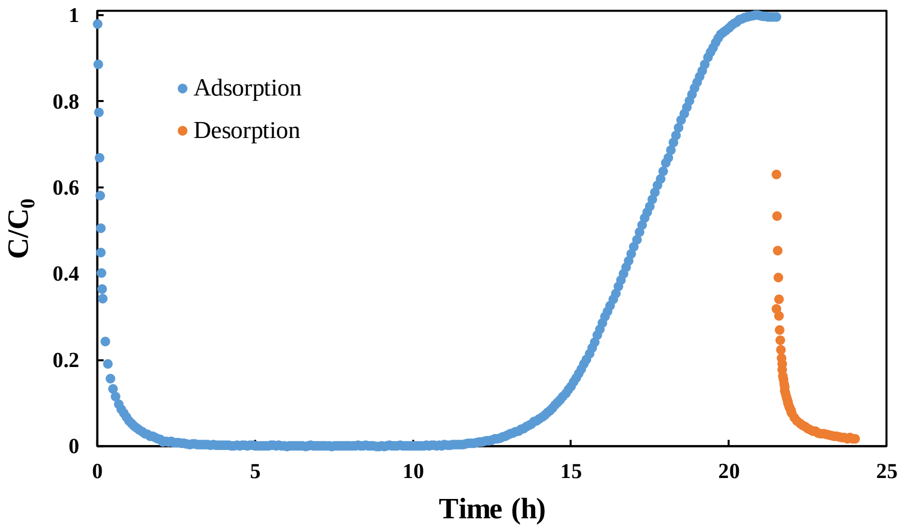

Figure 3 Adsorption of toluene in dry air (initial concentration=1000 ppm; total flow rate=0.1 L/min) and desorption of reversibly adsorbed toluene by dry air flushing (total flow rate=0.5 L/min) on NTP activated MS-13X

3.2.2 Oxidation of toluene adsorbed on NTP activated MS-13X

During the first 10-30 minutes of NTP exposure, as shown in Figure 4, a significant amount of the irreversibly adsorbed toluene is desorbed. The total amount of toluene desorbed during this period is 1.04 mmol/g which accounts for 44.6 % of the irreversibly adsorbed toluene after flushing with dry air. The toluene desorption by NTP discharge can be reduced by process optimization as follows: (i) optimizing the NTP operating parameters to reduce the amount of toluene desorbed at a given time and to increase ozone formation, (ii) optimizing the NTP reactor for ozone generation required for the deep oxidation of adsorbed toluene, and (iii) subsequent selective adsorption of desorbed unconverted toluene and conversion. The remaining 1.29 ± 0.03 mmol/g of toluene is converted during NTP exposure. The two main carbon containing gaseous by-products detected during NTP exposure are CO_2 and CO. As shown in Figure 4, the concentrations of CO and CO_2 start to increase steeply after 10 minutes of NTP exposure reaching a plateau after 20 minutes. After approximately 35 minutes of NTP exposure, the concentrations of CO_2 and CO start to decrease indicating a decrease in the amount of adsorbed toluene oxidized on the MS-13X surface. The total amount of CO_2 and CO formed are 1.90 mmol/g and 0.72 mmol/g, respectively, which result in a CO_2 and CO selectivity of 21.0 ± 0.4 % and 8.0 ± 0.2 %, respectively.

The FTIR spectra of the outlet gas during NTP treatment at three different exposure times (20, 40, and 60 minutes) are shown in Figure 5. Apart from the desorption of unconverted toluene and the formation of CO_2, CO and H_2O, there was also the formation of N_2O (Reaction 12) [34], at 40 and 60 minutes and the temporal evolution of N_2O is depicted in Figure 6(a). In addition, the formation of NO and NO_2 was also observed at 60 minutes of NTP exposure. In the temporal evolution of NO (shown in Figure 6(b)), NO is already formed after 40 minutes of NTP exposure. However, this NO formation is not visible in the FTIR spectrum due to the presence of a broad H_2O band which overlaps with the characteristic peaks of NO. The formation of NO is according to the Reaction 13 or the Reaction 14 [35], while NO_2 is formed through the oxidation of NO (Reactions 15 & 16) [36]. The increase in the concentration of N_2O and the presence of more electronically excited oxygen atoms result in the formation of NO after 40 minutes of NTP exposure. The formation of NO_2 after 50 minutes of NTP exposure is probably due to the availability of the atomic oxygen species and ozone, which were initially involved in the conversion of adsorbed toluene. As CSD provides the flexibility for the choice of discharge gas and considering the toxicity and negative environmental impact of oxides of nitrogen [37], the formation of these compounds can be avoided by using non-nitrogen gas such as O_2 diluted in He or Ar during the discharge stage. Ozone, which is one of the main oxygen species produced in a dry air plasma [26] was also detected in the outlet of the MS-13X pellets & glass beads packed bed DBD reactor, but only during the first 5 minutes of NTP exposure. The temporal evolution of O_3 (not shown here) showed an initial O_3 concentration of 200 ppm immediately after plasma ignition, which rapidly decreased to zero after five minutes of NTP exposure.

$$N_2(A^3 \textstyle\sum_u +) + O_2 \rightarrow N_2O + O \qquad 1$$

$$O(^1D) + N_2O \rightarrow 2NO \qquad 2$$

$$N(^2D) + O_2 \rightarrow NO + O(^3P) \qquad 3$$

$$NO + O + M \rightarrow NO_2 + M\ (M = N_2, O_2, NO, NO_2, N_2O) \qquad 4$$

$$NO + O_3 \rightarrow NO_2 + O_2 \qquad 5$$

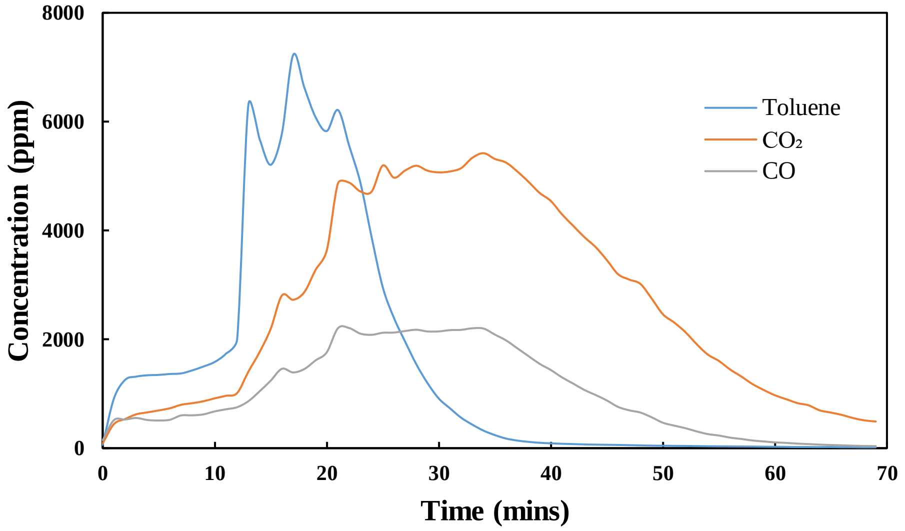

Figure 4 Temporal evolution of the concentration of desorbed toluene, CO_2 and CO formed during NTP exposure at the plasma reactor outlet (total flow rate=0.5 L/min; applied voltage=7.5 kV; discharge power=65 W)

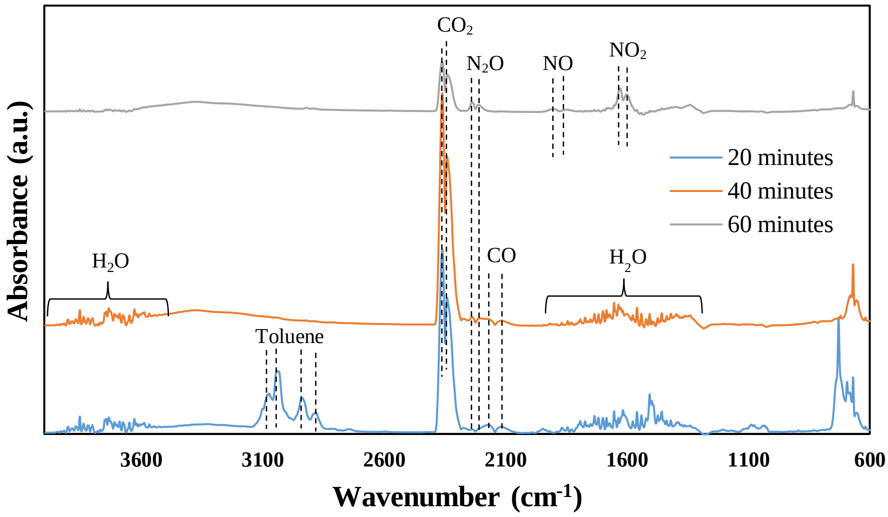

Figure 5 FTIR spectra of the plasma reactor outlet gas during NTP exposure of NTP activated MS-13X at three different times after NTP ignition (20, 40 and 60 minutes) (total flow rate=0.5 L/min; applied voltage=7.5 kV; discharge power=65 W)

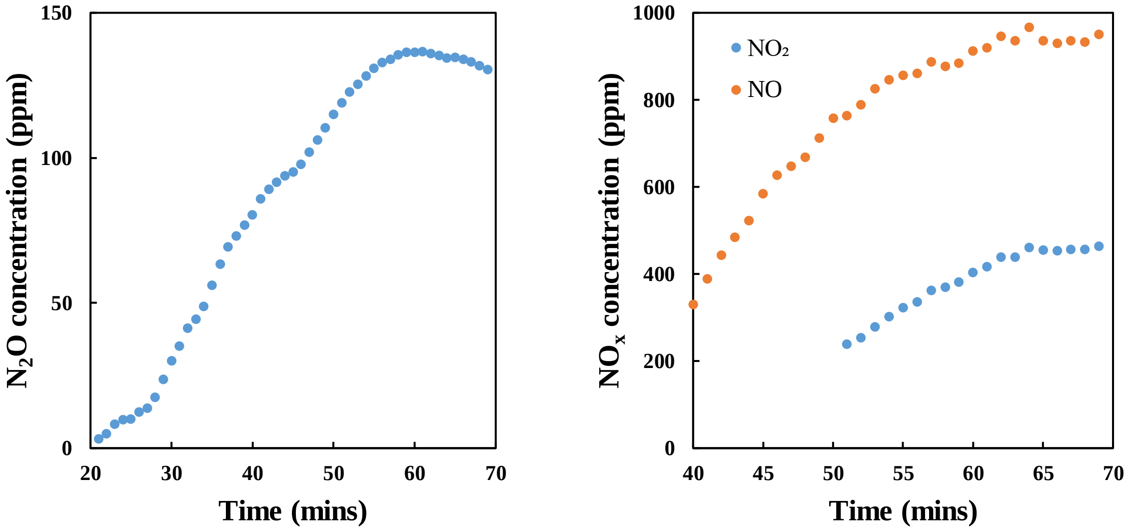

Figure 6 Temporal evolution of the concentration of different nitrogen containing by-products: (a) N_2O*, (b) NO and* NO_2 *during NTP exposure of NTP activated MS-13X*

3.2.3 Regeneration of 13X zeolite

The breakthrough curves of toluene adsorbed on NTP activated (fresh) and NTP (I) regenerated (used) MS-13X are shown in Figure 7. From Figure 7, it is determined that the total amount of toluene adsorbed on NTP (I) regenerated MS-13X is 2.49 ± 0.03 mmol/g, which is similar to that of the fresh NTP activated MS-13X. The critical concentration of toluene was also observed after 14.6 and 14.9 hours for NTP activated and NTP (I) regenerated MS-13X, respectively. These results demonstrate the complete regeneration of the used MS-13X after one cycle of CSD.

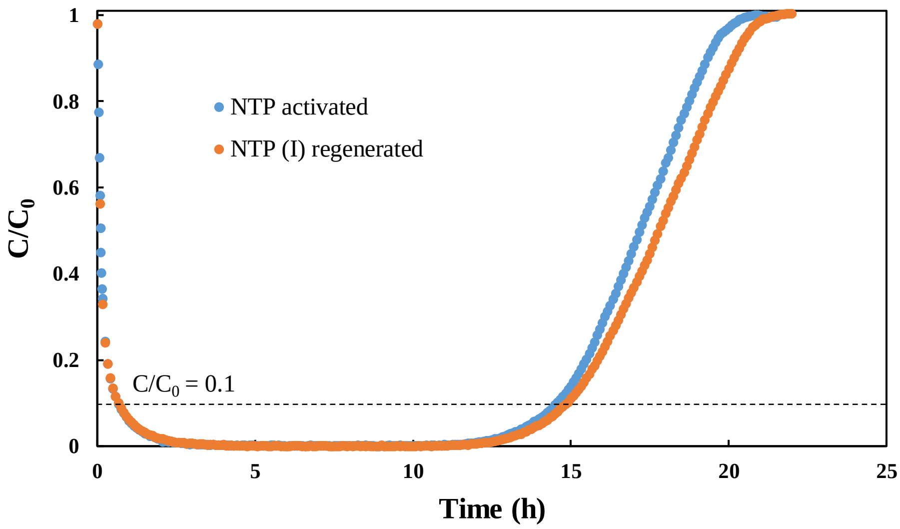

Figure 7 Breakthrough curves for the adsorption of toluene from dry air until saturation on NTP activated and NTP (I) regenerated MS-13X

In this work, the carbon balances were calculated by considering the total amount of toluene adsorbed as 100%. As shown in Figure 8 and Table S3, the amounts of toluene desorbed by the flushing of dry air for NTP activated and NTP (I) regenerated MS-13X are the same. On the other hand, the desorption of unconverted toluene by the NTP discharge for the NTP (I) regenerated MS-13X (43.8%) sample is slightly higher than the NTP activated MS-13X sample (42.4%), resulting in the same amount of toluene converted for both samples. Finally, the CO_x yield of the NTP (I) regenerated sample is lower than the NTP activated MS-13X, resulting in slightly more missing carbon for the former sample. The missing carbon for both zeolite samples could be explained by the presence of oil-like deposits on the inner wall of the plasma reactor outside the plasma discharge zone, which was also reported by other researchers even in the presence of transition metal oxide catalysts [38]. The formation of these deposits could be potentially reduced by heating the walls of the plasma reactor, by increasing the applied gas flow rate and by loading transition metal oxide on MS-13X [39]. To conclude, for the same amount of converted toluene, more CO_2 and CO are formed when using the NTP activated MS-13X compared to the NTP (I) regenerated MS-13X, consequently resulting in a higher CO_2 and CO selectivity for NTP activated MS-13X. On the other hand, the higher adsorption time on the NTP (I) regenerated MS-13X results in a lower energy cost to remedy 1 m^3 of air (Table 2), whereas the energy yield remains the same for both the MS-13X. The performance of APC/CSD process using MS-13X reported in various work are listed in Table 3. This overview highlights that comparable CO_x yield has been obtained in this work despite higher amount of toluene adsorbed on MS-13X and suggests that metal loading on MS-13X yields better selectivity towards CO_2 formation.

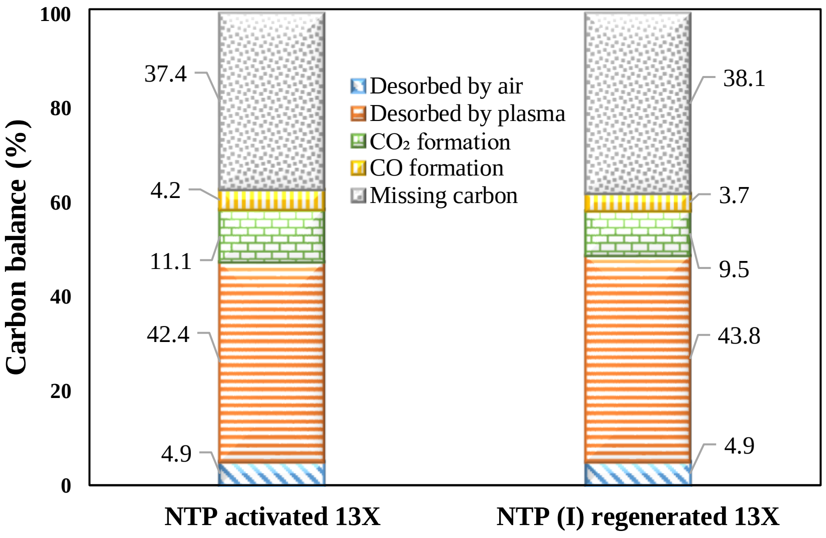

Figure 8 Carbon balance of the NTP activated and NTP (I) regenerated MS-13X

Table 2 CO_x yield, product selectivity, energy cost and energy yield for NTP activated and NTP (I) regenerated MS-13X

	NTP activated	**NTP (I) regenerated**
	MS-13X	
CO_x yield (%)	15.3 ± 0.3	13.2 ± 0.2
CO_2 selectivity (%)	21.0 ± 0.4	18.5 ± 0.2
CO selectivity (%)	8.0 ± 0.2	7.1 ± 0.1
CO_x selectivity (%)	29.0 ± 0.6	25.7 ± 0.3

Energy cost (kWhm^{-3})	0.60	0.55
Energy yield (g/kWh)	6.04 ± 0.13	6.13 ± 0.07

Table 3 Overview of reported work on toluene abatement by APC/CSD process using MS-13X

Adsorbent	Toluene adsorbed (mmol)	NTP reactor	Discharge gas	CO_x yield (%)	Regeneration	Ref.
MS-13X	2.45	DBD (ventilated)	Air	15	Yes	This work
MS-13X	0.57	DBD (ventilated)	Air	20	n.a.	[18]
MS-13X	0.57	DBD (closed)	Air	<5	n.a.	[19]
Co/MS-13X	0.51	DBD (ventilated)	Air	80	n.a.	[19]
Co/MS-13X	0.51	DBD (ventilated)	O_2	100	n.a.	[19]

3.3 Surface and bulk properties of activated and regenerated MS-13X

The surface and bulk properties of the thermal activated, NTP activated and NTP regenerated MS-13X are investigated in this section. To understand the effect of NTP exposure on the MS-13X properties and to establish correlations between the properties and its performance in APC process, the surface and bulk properties of the zeolite are measured.

As a first step, the PXRD patterns of the fresh, thermal activated, NTP activated and NTP (II) regenerated MS-13X are studied to examine the crystallinity of the samples after plasma exposure (shown in Figure 9). The fresh MS-13X sample is regarded as the reference sample for this particular study. The diffraction of the three samples match with those reported for the FAU structure of MS-13X (JCPDS card No. 38-0237) by other researchers [40–44]. Moreover, no shift in the diffractions and no significant diffraction lines corresponding to any new phase is observed after NTP exposure. This observation, together with the remaining high diffraction intensities and low background, clearly show that the crystallinity of MS-13X is maintained.

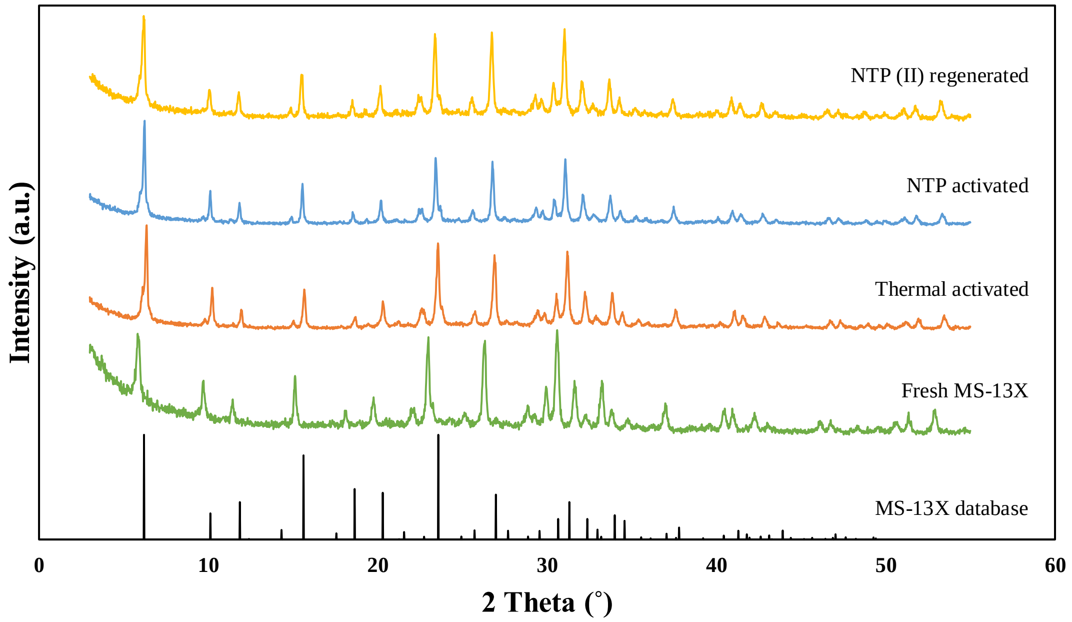

Figure 9 PXRD patterns of fresh, thermal activated, NTP activated and NTP (II) regenerated MS-13X

The XPS survey spectra of the thermal activated, NTP activated and NTP (II) regenerated MS-13X reveal the presence of the following elements: C, O, Na, Si, Al and Ca and the corresponding surface elemental composition is shown in Table 4. This analysis reveals that the examined zeolite samples have a similar surface elemental composition. It is known from literature that the adsorption capacity of zeolites changes as a function of their Si/Al ratio [45]. However, there is no difference in the surface Si/Al ratio of thermal and NTP activated MS-13X samples.

The high-resolution O1s & Al2p and C1s, Na1s & Si2p spectra of the thermal activated, NTP activated and NTP (II) regenerated MS-13X are shown in Figure 10 and Figure S4 respectively. The high-resolution C1s (either impurities or adsorbed carbonaceous compounds) spectra (Figure S4(a)) are deconvoluted into four photopeaks centred at 285.0, 286.4, 287.5 and 289.2 eV, which correspond to C-C, C-O, C=O and O-C=O bonds, respectively [46]. No significant differences are observed in the relative areas of these peaks for the three investigated zeolite samples suggesting that there is no deposition of carbon containing compounds (see Figure 8) from the CSD process. The high-resolution O1s region (shown in Figure 10(a)) are deconvoluted by using 4 photopeaks centred at 531.2, 532.3, 533.4 and 537 eV. The first photopeak at 531.2 eV corresponds to the oxygen present in the zeolite framework, whereas the photopeaks at 532.3 and 533.4 eV correspond to C=O and O=C-O bonds and the photopeak at 537 eV corresponds to Na KLL [47]. From the depicted O1s spectra, it can be seen that the oxygen percentage in the zeolite framework for the NTP activated (49.6 %) and the NTP (II) regenerated (50.0 %) MS-13X is higher than in case of the thermal activated MS-13X (45.0 %). This observation suggests that NTP activation of MS-13X desorbs the carbonaceous compounds (especially CO_2) more effectively. In addition, the ratio of the oxygen present in the zeolite framework (531.2 eV) to the adsorbed oxygen (532.3 and 533.4 eV) for NTP activated (1.05) and NTP (II) regenerated (1.06) MS-13X is similar, suggesting that there are no residual carbon containing compounds in the MS-13X after 2 cycles of CSD. Figure S4(b) depicts the Na1s spectra of the examined zeolites. In all samples, only one broad photopeak was observed at ~ 1072 eV, which can be assigned to Na_2O [48]. No shift in the Na1s peak of MS-13X was observed for any of the samples shows that the ionicity of the Na-O bonds was maintained after NTP exposure [49]. Figure S4(c) shows the high-resolution Si2p spectra of all the samples. These spectra are deconvoluted using 2 different peaks, which are centred at 103.4 eV and 102.4. The former peak can be attributed to the Si-O bonds in SiO_2, while the latter can be assigned to silicates. Moreover, there is no shift in the peak position of the Si-O bonds at 102.4 eV, suggesting that there is no change in the covalent nature of this bond due to plasma activation or cyclic CSD process [50]. In addition, there is also no shift in the peak which corresponds to silicates (peak centred at 103.4 eV). Finally, Figure 10(b) shows the Al2p spectra, which are deconvoluted using two peaks centred at 74.2 eV and 75.2 eV, that correspond to the Al-O bonds of Al_2O_3 and $Al(OH)_3$, respectively. From the Al2p spectra, the relative area of the peak centred at 75.2 eV (attributed to $Al(OH)_3$) in the NTP activated (18 %) and the NTP (II) regenerated (19 %) zeolite are similar to that of the thermal activated (16 %) MS-13X, which shows that there is no change in the presence of the EFAL species in MS-13X after NTP exposure.

Table 4 Surface elemental composition obtained from XPS survey spectra for thermal activated, NTP activated and NTP (II) regenerated MS-13X

	Atomic percentage (%)						
	C	O	Na	Al	Si	Ca	Si/Al
Thermal activated	9.0 ± 0.8	61.8 ± 0.4	6.4 ± 0.3	6.3 ± 0.0	15.6 ± 0.7	0.9 ± 0.1	2.5
NTP activated	9.4 ± 0.8	60.6 ± 1.1	6.3 ± 0.6	6.4 ± 0.6	15.7 ± 0.5	1.3 ± 0.1	2.4
NTP (II) regenerated	8.9 ± 0.6	61.7 ± 0.8	5.9 ± 0.2	6.3 ± 0.6	16.0 ± 0.4	1.2 ± 0.1	2.5

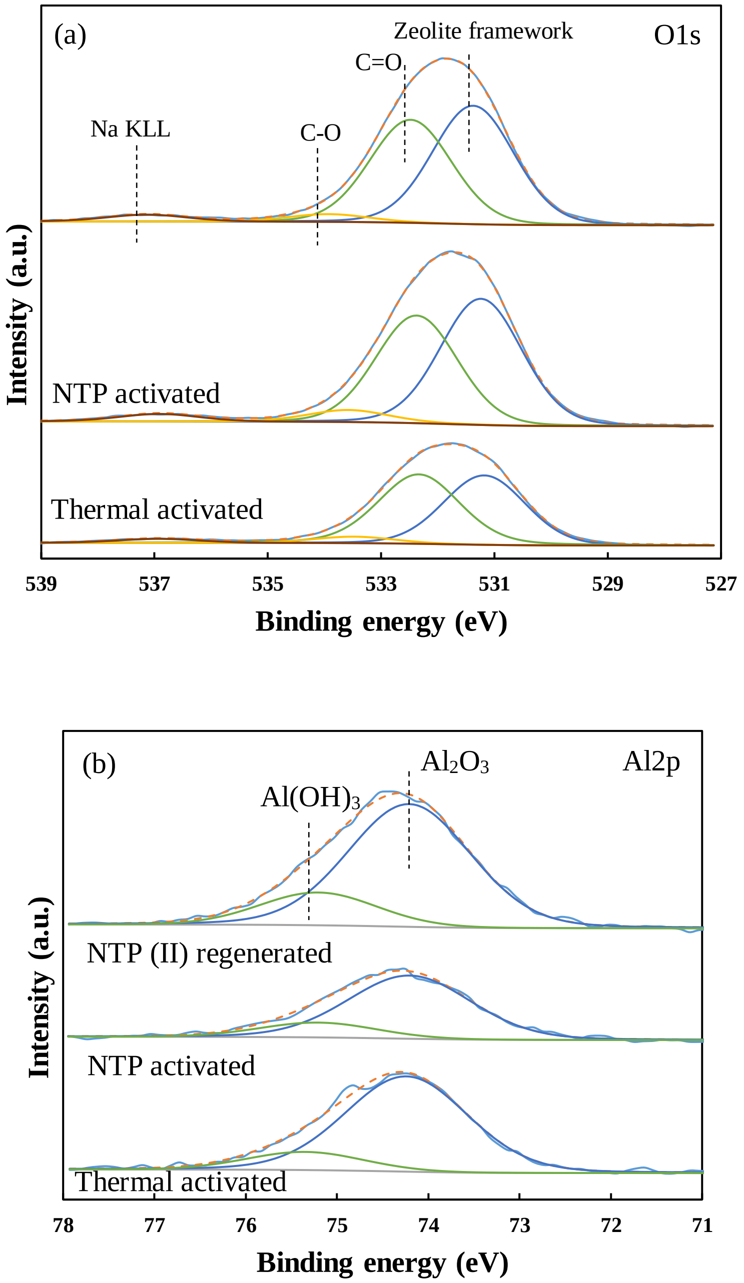

Figure 10 XPS high-resolution spectra of (a) O1s and (b) Al2p for thermal activated, NTP activated and NTP (II) regenerated MS-13X

The nitrogen adsorption-desorption isotherms of the fresh, thermal activated, NTP activated and NTP (II) regenerated MS-13X are shown in Figure S5(a). The isotherms of all samples belong to the type IV, in accordance with the IUPAC classification. At low relative pressure ($P/P_0 < 0.01$), the adsorbed volume sharply increases, after which a constant adsorbed volume in the relative pressure range of 0.1-0.6 is observed. The first increase is attributed to the filling of the micropores, whereas the second increase is visible at a relative pressure close to 1.0, which is probably due to the presence of macropores resulting from the use of binders and pore forming agents in the pelletization process. The specific surface area S_{BET} and pore volume of the four MS-13X samples are shown in Table 5. The results show that the S_{BET} of activated MS-13X is higher than the fresh MS-13X and there are no significant changes in the S_{BET} and pore volume after one-time (NTP activated) and three-times (NTP (II) regenerated) NTP exposure. The BJH (Barrett-Joyner-Halenda) pore size distribution (PSD) (Figure S5(b)) shows a broad distribution of mesopores (between 2 nm and 50 nm) for all samples. Additionally, there are no significant differences in PSD for the examined zeolites.

Although N_2 adsorption-desorption analysis is widely used to determine the surface properties, it is not suitable for the investigation of micropores in zeolites [51]. Thus, Ar was also used as an adsorbate for the analysis of the micropores in thermal and NTP activated MS-13X samples. The obtained Ar adsorption isotherms and the corresponding PSD are shown in Figure S6. The specific surface area (S_{BET}) of the NTP activated MS-13X is slightly lower in comparison to the thermal activated MS-13X (Table 5). The PSDs depicted in Figure S6(b) reveal a narrow distribution of micropores with a maximum around 1 nm.

Table 5 Surface properties of fresh, thermal activated, NTP activated and NTP regenerated MS-13X

	Fresh	Thermal activated	NTP activated	NTP (II) regenerated
S_{BET} (m^2/g) – N_2 sorption	312	347	352	347
Pore volume (ml/g) – N_2 sorption	0.10	0.24	0.24	0.24
S_{BET} (m^2/g) – Ar sorption	--	569	521	--

In order to investigate the effect of NTP exposure on the migration of aluminium from the framework, resulting in extra framework aluminium (EFAl), which are Lewis acid sites [52,53], *in-situ* IR spectroscopy of pyridine adsorbed on thermal and NTP activated MS-13X was performed. In addition, the analysis of the IR spectra of the OH groups were investigated to get more information about the nature of the acid sites. Figure S7(a) and (b) show the IR bands in the region 1570 – 1400 cm^{-1}. The two absorption bands observed in this region correspond to the C-C stretch of coordinatively bonded pyridine indicating the presence of Lewis acid sites (1445 cm^{-1}) and pyridine interacting with both Lewis and Brønsted acid sites (1490 cm^{-1}) [54]. On the other hand, the absorption peak corresponding to the stretching vibration of the pyridinium ion which is used to detect the Brønsted acid sites could not be seen in the obtained FTIR spectra [55,56]. Figure S7 also shows that with increasing the pyridine desorption temperature, the intensity of the bands at 1490 cm^{-1} and 1445 cm^{-1} decreases for both zeolites, which proves that mainly weak acidic sites are present in both MS-13X samples. The surface concentration of Lewis acid sites (Figure 11) clearly shows that the type and amount of acid sites is similar on the thermal and NTP activated zeolite for all examined desorption temperatures and there is no change in the amount of Lewis acid sites after NTP exposure. Figure S8 shows the IR bands in the region 3850 – 3550 cm^{-1} at pyridine desorption temperature of 450 ˚C. In both the samples, the band around 3740 cm^{-1} is attributed to surface silanols groups terminating the exterior of the crystal and the band around 3675 cm^{-1} is attributed to an OH group on EFAl species [57].

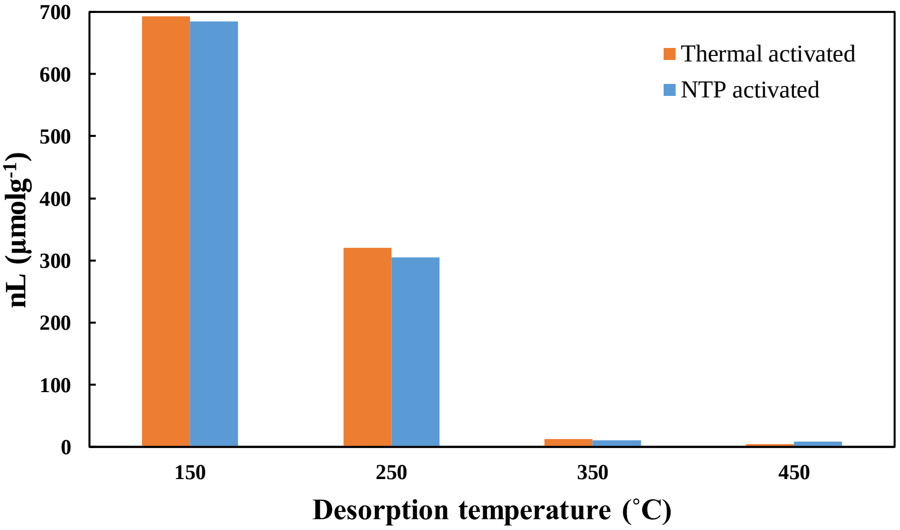

Figure 11 Evolution of the amount of Lewis acid sites as a function of the pyridine desorption temperature for thermal activated and NTP activated MS-13X

3.4 Reaction mechanism for the oxidation of toluene adsorbed on MS-13X

The exact adsorption mechanism of basic VOCs such as toluene on zeolites is still under debate but it has already been reported that toluene can be adsorbed both on the Lewis and Brønsted acid sites [58]. Based on the characterization of the acid sites performed in this study and on the OES measurement in our previous study [26], the plausible reaction mechanism for toluene oxidation is proposed. The adsorption of toluene on MS-13X is dominated by the formation of Lewis acid-base adducts. During NTP exposure, decomposition of adsorbed toluene occurs (i) in the gas phase for the desorbed toluene and (ii) on the surface of the MS-13X for the irreversibly adsorbed toluene. As the reaction mechanism of toluene oxidation in the gas phase is already well explained in literature, the reader is referred to an earlier study [9]. On the other hand, the decomposition of toluene on the surface of MS-13X proceeds by the following reactions:

$$O_3 + * \rightarrow O_3^* \tag{6}$$

$$O_3^* \rightarrow O^* + O_2 \tag{7}$$

$$O_3^* + O^* \rightarrow O_2^* + O_2 \tag{8}$$

$$O_2^* \rightarrow O_2 + * \tag{9}$$

where * represents the surface active sites, O_3^* is ozone adsorbed on the zeolite and O_2^* and O_2 are the surface oxide species. The adsorption and decomposition of ozone on MS-13X (Reactions 17 and 18) are due to the presence of Lewis acid sites [56,60], which was already confirmed by the pyridine FTIR study. Before switching on the NTP, the saturation of the MS-13X with toluene could occupy all available Lewis acid sites, which in turn explains the presence of ozone in the exit of the NTP reactor for the first five minutes of NTP exposure (Section 3.2.2). Afterwards, the desorption of toluene by NTP exposure (see Figure 4) makes some Lewis acid sites available for the adsorption and decomposition of ozone, which generates active oxygen species, which in turn react with adsorbed toluene. This explains the steep increase in the formation of CO_2 and CO after 10 minutes of NTP exposure (see Figure 4) by the following reaction:

$$C_6H_5CH_3 + 18O \rightarrow xCO_2 + yCO + H_2O + \textit{missing carbon} \tag{10}$$

3.5 Stability of MS-13X for cyclic adsorption-plasma catalysis

In this work, the stability of the NTP activated MS-13X was analyzed by saturating MS-13X until the critical outlet concentration of toluene for 10 cycles of the CSD process. The carbon balance, the total amount of adsorbed toluene, the regeneration efficiency and the product (CO_2 and CO_x) selectivity are shown in Figure 12 and Table S4. The total amount of adsorbed toluene during 10 cycles was in the range 1.8 - 1.9 mmol/g which demonstrates that the NTP exposure completely regenerates the MS-13X. The amount of toluene desorbed by flushing air and the amount of toluene desorbed by NTP exposure was similar for all cycles. The regeneration efficiency is higher than 97% for all 10 cycles (Table S4). In addition, the CO_2 and CO_x selectivities also remain constant at approximately 25.6 ± 1.0 % and 35.4 ± 1.4 %, respectively. These experimental results suggest that the MS-13X is stable during 10 cycles of NTP exposure, or in other words, the applied CSD technique is a promising process for the removal of toluene from air and the regeneration of the used MS-13X.

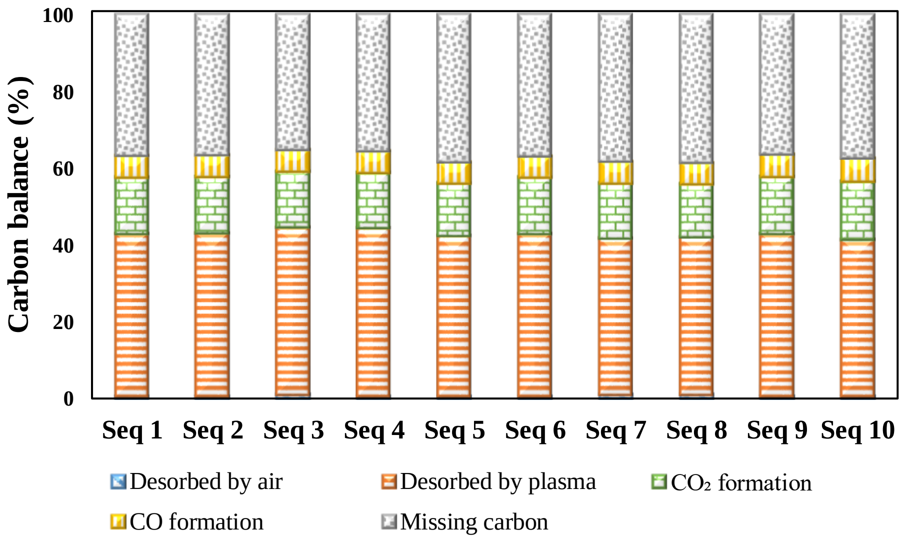

Figure 12 Carbon balance for the adsorption plasma catalytic abatement of toluene adsorbed until the critical concentration on NTP activated and NTP regenerated MS-13X for 10 cycles

4. Conclusion

This work investigates the use of non-thermal plasma for the activation and regeneration of MS-13X pellets during CSD of toluene. The NTP activation of MS-13X by NTP results in a higher toluene adsorption when compared to the thermal activation. Analysis of the surface and bulk properties of thermal activated and NTP activated MS-13X shows that the crystallinity, pore volume, pore size distribution, type and amount of acid sites and elemental composition are not altered by the plasma discharge.

The regeneration of MS-13X by NTP exposure is also demonstrated in this study by comparing the amount of adsorbed toluene, and by determining the catalytic activity using fresh NTP activated and used NTP regenerated MS-13X for the CSD removal of toluene. The amount of toluene adsorbed on both MS-13X samples remains unaltered, whereas the CO_x yield is marginally reduced for the NTP regenerated MS-13X. Analysis of the bulk and surface properties of the fresh NTP activated and used NTP regenerated MS-13X reveals no significant difference between both samples, suggesting complete regeneration of the MS-13X by NTP exposure. Finally, a study on the stability and regeneration efficiency of MS-13X by NTP exposure for 10 cycles of CSD removal of toluene shows a complete regeneration of the used MS-13X.

This work thus clearly demonstrates that the use of MS-13X for the CSD elimination of toluene fulfils the following criteria: (i) an improved ratio of adsorption time to NTP exposure time, thus a reduced energy cost of the process, (ii) stability of the MS-13X in the discharge and (iii) regenerability of the MS-13X by NTP exposure. Unfortunately, there was no total oxidation of toluene, resulting in missing carbon and CO formation which corresponds to 42% of the total adsorbed carbon, irrespective of the initial amount of adsorbed toluene. This implies that further work has to be done to enhance the total toluene oxidation either by engineering the adsorbent or by process optimization.

Acknowledgments

The project “DepollutAir” funded by the European Program INTERREG V France-Wallonie-Flanders FEDER is acknowledged for supporting and funding this research work (grant number 1.1.18). This research was carried out in the French-Belgium Associated International Laboratory "Plasma & Catalysis" supported by the University of Lille and Ghent University.

References

[1] C.O. Baltaretu, E.I. Lichtman, A.B. Hadler, M.J. Elrod, Primary atmospheric oxidation mechanism for toluene, The Journal of Physical Chemistry A. 113 (2009) 221–230. https://doi.org/10.1021/jp806841t.

[2] F.I. Khan, A. Kr. Ghoshal, Removal of Volatile Organic Compounds from polluted air, Journal of Loss Prevention in the Process Industries. 13 (2000) 527–545. https://doi.org/10.1016/S0950-4230(00)00007-3.

[3] A.M. Vandenbroucke, R. Morent, N. De Geyter, C. Leys, Non-thermal plasmas for non-catalytic and catalytic VOC abatement, J Hazard Mater. 195 (2011) 30–54. https://doi.org/10.1016/j.jhazmat.2011.08.060.

[4] F. Gironi, V. Piemonte, VOCs removal from dilute vapour streams by adsorption onto activated carbon, Chemical Engineering Journal. 172 (2011) 671–677. https://doi.org/10.1016/j.cej.2011.06.034.

[5] F. Salvador, N. Martin-Sanchez, R. Sanchez-Hernandez, M.J. Sanchez-Montero, C. Izquierdo, Regeneration of carbonaceous adsorbents. Part II: Chemical, Microbiological and Vacuum Regeneration, Microporous and Mesoporous Materials. 202 (2015) 277–296. https://doi.org/10.1016/j.micromeso.2014.08.019.

[6] F. Salvador, N. Martin-Sanchez, R. Sanchez-Hernandez, M.J. Sanchez-Montero, C. Izquierdo, Regeneration of carbonaceous adsorbents. Part I: Thermal Regeneration, Microporous and Mesoporous Materials. 202 (2015) 259–276. https://doi.org/10.1016/j.micromeso.2014.02.045.

[7] K.-J. Kim, H.-G. Ahn, The effect of pore structure of zeolite on the adsorption of VOCs and their desorption properties by microwave heating, Microporous and Mesoporous Materials. 152 (2012) 78–83. https://doi.org/10.1016/j.micromesa.2011.11.051.

[8] Z.-Z. Xie, L. Wang, G. Cheng, L. Shi, Y.-B. Zhang, Adsorption properties of regenerative materials for removal of low concentration of toluene, J Air Waste Manage Assoc. 66 (2016) 1224–1236. https://doi.org/10.1080/10962247.2016.1209257.

[9] S.K.P. Veerapandian, J.-M. Giraudon, N. De Geyter, Y. Onyshchenko, C. Krishnaraj, S. Sonar, A. Löfberg, K. Leus, P. Van Der Voort, J.-F. Lamonier, R. Morent, Regeneration of Hopcalite used for the adsorption plasma catalytic removal of toluene by non-thermal plasma, Journal of Hazardous Materials. (2020) 123877. https://doi.org/10.1016/j.jhazmat.2020.123877.

[10] L.Y. Jia, A. Farouha, L. Pinard, S. Hedan, J.D. Comparot, A. Dufour, K. Ben Tayeb, H. Vezin, C. Batiot-Dupeyrat, New routes for complete regeneration of coked zeolite, Applied Catalysis B: Environmental. 219 (2017) 82–91. https://doi.org/10.1016/j.apcatb.2017.07.040.

[11] S.K.P. Veerapandian, N. De Geyter, J.M. Giraudon, J.F. Lamonier, R. Morent, The use of zeolites for VOCs abatement by combining non-thermal plasma, adsorption, and/or catalysis: A review, Catalysts. 9 (2019). https://doi.org/10.3390/catal9010098.

[12] E. Van Bavel, V. Meynen, P. Cool, K. Lebeau, E.F. Vansant, Adsorption of hydrocarbons on mesoporous SBA-15 and PHTS materials, Langmuir. 21 (2005) 2447–2453. https://doi.org/10.1021/la0474417.

[13] M. Ghafari, J.D. Atkinson, Impact of styrenic polymer one-step hyper-cross-linking on volatile organic compound adsorption and desorption performance, Journal of Hazardous Materials. 351 (2018) 117–123. https://doi.org/10.1016/j.jhazmat.2018.02.051.

[14] F. Noël, C.A. Serra, S. Le Calvé, micromachines Design of a Novel Axial Gas Pulses Micromixer and Simulations of its Mixing Abilities via Computational Fluid Dynamics, (2019). https://doi.org/10.3390/mi10030205.

[15] I. Tsukada, S. Higuchi, Pulsed-laser deposition of $LiNbO_3$ in low gas pressure using pure ozone e, Japanese Journal of Applied Physics. 43 (2004) 5307. https://doi.org/10.1143/JJAP.43.5307.

[16] C.Y.H. Chao, C.W. Kwong, K.S. Hui, Potential use of a combined ozone and zeolite system for gaseous toluene elimination, Journal of Hazardous Materials. 143 (2007) 118–127. https://doi.org/10.1016/j.jhazmat.2006.08.077.

[17] J. Van Durme, J. Dewulf, W. Sysmans, C. Leys, H. Van Langenhove, Abatement and degradation pathways of toluene in indoor air by positive corona discharge, Chemosphere. 68 (2007) 1821–1829. https://doi.org/10.1016/j.chemosphere.2007.03.053.

[18] H. Yi, X. Yang, X. Tang, S. Zhao, J. Wang, X. Cui, T. Feng, Y. Ma, Removal of toluene from industrial gas over 13X zeolite supported catalysts by adsorption-plasma catalytic process, Journal of Chemical Technology and Biotechnology. 92 (2017) 2276–2286. https://doi.org/10.1002/jctb.5314.

[19] H. Yi, X. Yang, X. Tang, S. Zhao, Removal of toluene from industrial gas by adsorption–plasma catalytic process : Comparison of closed discharge and ventilated discharge, Plasma Chemistry and Plasma Processing. 38 (2018) 331–345. https://doi.org/10.1007/s11090-017-9863-1.

[20] Q.H. Trinh, S.B. Lee, Y.S. Mok, Removal of ethylene from air stream by adsorption and plasma-catalytic oxidation using silver-based bimetallic catalysts supported on zeolite, Journal of Hazardous Materials. 285 (2015) 525–534. https://doi.org/10.1016/j.jhazmat.2014.12.019.

[21] Q.H. Trinh, Y.S. Mok, Effect of the adsorbent/catalyst preparation method and plasma reactor configuration on the removal of dilute ethylene from air stream, Catalysis Today. 256 (2015) 170–177. https://doi.org/10.1016/j.cattod.2015.01.027.

[22] H.H. Kim, J.H. Kim, A. Ogata, Adsorption and oxygen plasma-driven catalysis for total oxidation of VOCs, International Journal of Plasma Environmental Science & Technology. 2 (2008) 106–112. https://doi.org/10.34343/ijpest.2008.02.02.106.

[23] H.H. Kim, A. Ogata, S. Futamura, Oxygen partial pressure-dependent behavior of various catalysts for the total oxidation of VOCs using cycled system of adsorption and oxygen plasma, Applied Catalysis B: Environmental. 79 (2008) 356–367. https://doi.org/10.1016/j.apcatb.2007.10.038.

[24] K. Shang, J. Ren, Q. Zhang, N. Lu, N. Jiang, J. Li, Successive treatment of benzene and derived byproducts by a novel plasma catalysis-adsorption process, Journal of Environmental Chemical Engineering. 9 (2021) 105767. https://doi.org/10.1016/J.JECE.2021.105767.

[25] S. Li, X. Yu, X. Dang, P. Wang, X. Meng, Q. Wang, H. Hou, Double dielectric barrier discharge incorporated with CeO2-Co3O4/γ-Al2O3 catalyst for toluene abatement by a sequential

adsorption–discharge plasma catalytic process, Journal of Cleaner Production. 340 (2022) 130774. https://doi.org/10.1016/J.JCLEPRO.2022.130774.

[26] Z. Ye, S.K.P. Veerapandian, I. Onyshchenko, A. Nikiforov, N. De Geyter, J.-M. Giraudon, J.-F. Lamonier, R. Morent, An in-Depth Investigation of Toluene Decomposition with a Glass Beads-Packed Bed Dielectric Barrier Discharge Reactor, Industrial and Engineering Chemistry Research. 56 (2017). https://doi.org/10.1021/acs.iecr.7b00963.

[27] G. Swetha, T. Gopi, S. Chandra Shekar, C. Ramakrishna, B. Saini, P.V.L. Rao, Combination of adsorption followed by ozone oxidation with pressure swing adsorption technology for the removal of VOCs from contaminated air streams, Chemical Engineering Research and Design. 117 (2017) 725–732. https://doi.org/10.1016/j.cherd.2016.11.036.

[28] S. Huang, W. Deng, L. Zhang, D. Yang, Q. Gao, Z. Tian, L. Guo, T. Ishihara, Adsorptive properties in toluene removal over hierarchical zeolites, Microporous and Mesoporous Materials. 302 (2020) 110204. https://doi.org/10.1016/j.micromeso.2020.110204.

[29] G. Qin, L. Zheng, Y. Xie, C. Wu, On the framework hydroxyl groups of H-ZSM-5 zeolites, Journal of Catalysis. 95 (1985) 609–612. https://doi.org/10.1016/0021-9517(85)90140-X.

[30] F. Holzer, U. Roland, F.D. Kopinke, Combination of non-thermal plasma and heterogeneous catalysis for oxidation of volatile organic compounds. Part 1. Accessibility of the intra-particle volume, Applied Catalysis B: Environmental. 38 (2002) 163–181. https://doi.org/10.1016/S0926-3373(02)00040-1.

[31] F. Zhang, A.C. Co, L. Olander, E. Wollenberg, F. Tubiello, J. Amouroux, S. Cavadias, A. Doubla, Carbon Dioxide reduction by non-equilibrium electrocatalysis plasma reactor, (n.d.). https://doi.org/10.1088/1757-899X/19/1/012005.

[32] R. V. Siriwardane, M.-S. Shen, E.P. Fisher, J. Losch, Adsorption of CO_2 on Zeolites at Moderate Temperatures, Energy & Fuels. 19 (2005) 1153–1159. https://doi.org/10.1021/ef040059h.

[33] P.J.E. Harlick, F.H. Tezel, An experimental adsorbent screening study for CO_2 removal from N_2, Microporous and Mesoporous Materials. 76 (2004) 71–79. https://doi.org/10.1016/j.micromeso.2004.07.035.

[34] X. Fan, S. Kang, J. Li, T. Zhu, Formation of Nitrogen Oxides (N_2O, NO, and NO_2) in Typical Plasma and Plasma-Catalytic Processes for Air Pollution Control, Water, Air, and Soil Pollution. 229 (2018) 1–12. https://doi.org/10.1007/s11270-018-4011-y.

[35] K. Krawczyk, Conversion of nitrous oxide by positive pulsed corona discharge, IEEE Transactions on Plasma Science. 37 (2009) 884–889. https://doi.org/10.1109/TPS.2009.2018261.

[36] S. Pekárek, Effect of catalysts on dc corona discharge poisoning, European Physical Journal D. 61 (2011) 657–662. https://doi.org/10.1140/epjd/e2010-10246-4.

[37] L.W. Stanek, J.S. Brown, Air Pollution: Sources, Regulation, and Health Effects, Reference Module in Biomedical Sciences. (2019). https://doi.org/10.1016/B978-0-12-801238-3.11384-4.

[38] J. Li, H. Zhang, D. Ying, Y. Wang, T. Sun, J. Jia, In Plasma Catalytic Oxidation of Toluene Using Monolith CuO Foam as a Catalyst in a Wedged High Voltage Electrode Dielectric Barrier Discharge Reactor: Influence of Reaction Parameters and

Byproduct Control, International Journal of Environmental Research and Public Health. 16 (2019) 711. https://doi.org/10.3390/ijerph16050711.

[39] O. Karatum, M.A. Deshusses, A comparative study of dilute VOCs treatment in a non-thermal plasma reactor, Chemical Engineering Journal. 294 (2016) 308–315. https://doi.org/10.1016/j.cej.2016.03.002.

[40] C. Zhao, H. Deng, Y. Li, Z. Liu, Photodegradation of oxytetracycline in aqueous by 5A and 13X loaded with TiO_2 under UV irradiation, Journal of Hazardous Materials. 176 (2010) 884–892. https://doi.org/10.1016/j.jhazmat.2009.11.119.

[41] M.M.J. Treacy, J.B. Higgins, Collection of simulated XRD powder patterns for zeolites, 2007.

[42] C. Ramakrishna, B.K. Saini, K. Racharla, S. Gujarathi, C.S. Sridara, A. Gupta, G. Thakkallapalli, P.V.L. Rao, Rapid and complete degradation of sulfur mustard adsorbed on M/zeolite-13X supported (M = 5 wt% Mn, Fe, Co) metal oxide catalysts with ozone, RSC Advances. 6 (2016) 90720–90731. https://doi.org/10.1039/c6ra17215f.

[43] K.M. Valkaj, A. Katović, S. Zrnčević, Catalytic properties of Cu/13X zeolite based catalyst in catalytic wet peroxide oxidation of phenol, Industrial and Engineering Chemistry Research. 50 (2011) 4390–4397. https://doi.org/10.1021/ie102223g.

[44] C. Zhou, A. Alshameri, C. Yan, X. Qiu, H. Wang, Y. Ma, Characteristics and evaluation of synthetic 13X zeolite from Yunnan's natural halloysite, Journal of Porous Materials. 20 (2013) 587–594. https://doi.org/10.1007/s10934-012-9631-9.

[45] M.A. Hernández, L. Corona, A.I. Gonzalez, F. Rojas, V.H. Lara, F. Silva, Quantitative study of the adsorption of aromatic hydrocarbons (benzene, toluene, and p-xylene) on dealuminated clinoptilolites, Industrial and Engineering Chemistry Research. 44 (2005) 2908–2916. https://doi.org/10.1021/ie049276w.

[46] P.S. Esbah Tabaei, R. Ghobeira, P. Cools, F. Rezaei, A. Nikiforov, R. Morent, N. de Geyter, Comparative study between in-plasma and post-plasma chemical processes occurring at the surface of UHMWPE subjected to medium pressure Ar and N2 plasma activation, Polymer (Guildf). (2020) 122383. https://doi.org/10.1016/j.polymer.2020.122383.

[47] V.H. Ramos-Martinez, E. Ramirez-Vargas, F.J. Medellin-Rodriguez, C.A. Ávila-Orta, C.A. Gallardo-Vega, A.B. Jasso-Salcedo, M.L. Andrade-Guel, Zeolite 13X modification with gamma-aminobutyric acid (GABA), Microporous and Mesoporous Materials. 295 (2020) 109941. https://doi.org/10.1016/j.micromeso.2019.109941.

[48] R. Vinodh, C. Deviprasath, C.V.V. Muralee Gopi, V.G. Raghavendra Kummara, R. Atchudan, T. Ahamad, H.J. Kim, M. Yi, Novel 13X Zeolite/PANI electrocatalyst for hydrogen and oxygen evolution reaction, International Journal of Hydrogen Energy. (2020). https://doi.org/10.1016/j.ijhydene.2020.07.194.

[49] T.L. Barr, The nature of the relative bonding chemistry in zeolites: An XPS study, Zeolites. 10 (1990) 760–765. https://doi.org/10.1016/0144-2449(90)90058-Y.

[50] X. Wang, C.A. Plackowski, A. V. Nguyen, X-ray photoelectron spectroscopic investigation into the surface effects of sulphuric acid

treated natural zeolite, Powder Technology. 295 (2016) 27–34. https://doi.org/10.1016/j.powtec.2016.03.025.

[51] K.A. Cychosz, R. My Guillet-Nicolas, J. Garcí A-Martí Nez, M. Thommes, Recent advances in the textural characterization of hierarchically structured nanoporous materials, Chem. Soc. Rev. 46 (2017) 389. https://doi.org/10.1039/c6cs00391e.

[52] Z. Wang, L.A. O'Dell, X. Zeng, C. Liu, S. Zhao, W. Zhang, M. Gaborieau, Y. Jiang, J. Huang, Insight into Three-Coordinate Aluminum Species on Ethanol-to-Olefin Conversion over ZSM-5 Zeolites, Angewandte Chemie. 131 (2019) 18229–18236. https://doi.org/10.1002/ange.201910987.

[53] G. Li, E.A. Pidko, The Nature and Catalytic Function of Cation Sites in Zeolites: a Computational Perspective, ChemCatChem. 11 (2019) 134–156. https://doi.org/10.1002/cctc.201801493.

[54] L.P. Teh, S. Triwahyono, A.A. Jalil, R.R. Mukti, M.A.A. Aziz, T. Shishido, Mesoporous ZSM5 having both intrinsic acidic and basic sites for cracking and methanation, Chemical Engineering Journal. 270 (2015) 196–204. https://doi.org/10.1016/j.cej.2015.01.084.

[55] F. Jin, Y. Li, A FTIR and TPD examination of the distributive properties of acid sites on ZSM-5 zeolite with pyridine as a probe molecule, Catalysis Today. 145 (2009) 101–107. https://doi.org/10.1016/j.cattod.2008.06.007.

[56] S. Alejandro, H. Valdés, M.H. Manéro, C.A. Zaror, Oxidative regeneration of toluene-saturated natural zeolite by gaseous ozone: The influence of zeolite chemical surface characteristics, Journal of Hazardous Materials. 274 (2014) 212–220. https://doi.org/10.1016/j.jhazmat.2014.04.006.

[57] S. Schallmoser, T. Ikuno, M.F. Wagenhofer, R. Kolvenbach, G.L. Haller, M. Sanchez-Sanchez, J.A. Lercher, Impact of the local environment of Brønsted acid sites in ZSM-5 on the catalytic activity in n-pentane cracking, Journal of Catalysis. 316 (2014) 93–102. https://doi.org/10.1016/j.jcat.2014.05.004.

[58] H. Valdés, V.A. Solar, E.H. Cabrera, A.F. Veloso, C.A. Zaror, Control of released volatile organic compounds from industrial facilities using natural and acid-treated mordenites: The role of acidic surface sites on the adsorption mechanism, Chemical Engineering Journal. 244 (2014) 117–127. https://doi.org/10.1016/j.cej.2014.01.044.

[59] Z. Ye, S.K.P. Veerapandian, I. Onyshchenko, A. Nikiforov, N. de Geyter, J.-M. Giraudon, J.-F. Lamonier, R. Morent, An in-Depth Investigation of Toluene Decomposition with a Glass Beads-Packed Bed Dielectric Barrier Discharge Reactor, Industrial and Engineering Chemistry Research. 56 (2017). https://doi.org/10.1021/acs.iecr.7b00963.

[60] T. Yin, X. Meng, L. Jin, C. Yang, N. Liu, L. Shi, Prepared hydrophobic Y zeolite for adsorbing toluene in humid environment, Microporous and Mesoporous Materials. 305 (2020) 110327. https://doi.org/10.1016/j.micromeso.2020.110327.